

THE 3-DIMENSIONAL ARCHITECTURE OF THE ν ANDROMEDAE PLANETARY SYSTEM

RUSSELL DEITRICK

Department of Astronomy, University of Washington, Seattle, WA 98195-1580, USA

RORY BARNES

Department of Astronomy, University of Washington, Seattle, WA 98195-1580, USA

BARBARA MCARTHUR

Department of Astronomy, University of Texas at Austin, TX 78712, USA

THOMAS R. QUINN

Department of Astronomy, University of Washington, Seattle, WA 98195-1580, USA

RODRIGO LUGER

Department of Astronomy, University of Washington, Seattle, WA 98195-1580, USA

ADRIENNE ANTONSEN

Department of Astronomy, University of Washington, Seattle, WA 98195-1580, USA

AND

G. FRITZ BENEDICT

Department of Astronomy, University of Texas at Austin, TX 78712, USA

(Dated:)

Draft version August 14, 2018

ABSTRACT

The Upsilon Andromedae system is the first exoplanetary system to have the relative inclination of two planets’ orbital planes directly measured, and therefore offers our first window into the 3-dimensional configurations of planetary systems. We present, for the first time, full 3-dimensional, dynamically stable configurations for the 3 planets of the system consistent with all observational constraints. While the outer 2 planets, c and d, are inclined by $\sim 30^\circ$, the inner planet’s orbital plane has not been detected. We use N-body simulations to search for stable 3-planet configurations that are consistent with the combined radial velocity and astrometric solution. We find that only 10 trials out of 1000 are robustly stable on 100 Myr timescales, or ~ 8 billion orbits of planet b. Planet b’s orbit must lie near the invariable plane of planets c and d, but can be either prograde or retrograde. These solutions predict b’s mass is in the range 2 - 9 M_{Jup} and has an inclination angle from the sky plane of less than 25° . Combined with brightness variations in the combined star/planet light curve (“phase curve”), our results imply that planet b’s radius is $\sim 1.8 R_{Jup}$, relatively large for a planet of its age. However, the eccentricity of b in several of our stable solutions reaches > 0.1 , generating upwards of 10^{19} watts in the interior of the planet via tidal dissipation, possibly inflating the radius to an amount consistent with phase curve observations.

Subject headings: planetary systems, planets and satellites: dynamical evolution and stability, stars: individual (Upsilon Andromedae)

1 INTRODUCTION

1.1 Observations

The ν Andromedae (ν And) planetary system was the first discovered multi-exoplanet system around a main sequence star and is possibly still the most studied multi-planet system other than our Solar System. ν And b was discovered using the radial velocity (RV) technique by Butler et al. (1997) at Lick observatory. Two years later, combined data from Lick and the Advanced Fiber-Optic Echelle spectrometer (AFOE) at Whipple Observatory

revealed the presence of two additional planets, ν And c and d (Butler et al. 1999). Follow-up by François et al. (1999) confirmed that the existence of planets was the best explanation for the RV variations. Even at the time of Butler et al. (1999), the semi-major axes of the planets (0.059, 0.83, and 2.5 au), the minimum masses (0.71, 2.11, and 4.61 M_{Jup}), and eccentricities (0.034, 0.18, and 0.41) made it clear that this system was very unlike our Solar System, and it has presented a challenge to planet formation models that explain the Solar System. Stepinski et al. (2000) confirmed the presence of these three RV signatures in the existing data using two different fitting algorithms, but stressed that the eccentricity of planet c

was poorly constrained by the existing data.

Thus far, astrometry is one of the few techniques that can be used to break the $m \sin i$ degeneracy in the RV method for non-transiting planets (the other is a relatively new technique that uses high-resolution spectra to directly observe the radial velocity of the planet; for example, see Brogi et al. 2012; Rodler et al. 2012). Astrometry is the process of measuring a star’s movement on the plane of the sky, and hence provides 2-dimensional information which is orthogonal to RV. Because this measurement is made relative to other objects in the sky, it is extremely difficult to obtain the high precision necessary to detect planets. For small, close-in planets, the necessary precision is in the μas range (Quirrenbach 2010), since astrometry is more sensitive to planets with relatively large mass, low inclination and large semi-major axis. Nonetheless, Mazeh et al. (1999) reported a small, positive detection in the HIP data of an astrometric signal at the period of planet d, and derived an inclination of 156° and a mass of $10.1 M_{Jup}$. However, Pourbaix (2001) demonstrated that astrometric fits to the HIP data for 42 stars, including v And, were not significantly improved by the inclusion of a planetary orbit, and that the inclinations for planets c and d could be statistically rejected. Reffert & Quirrenbach (2011) re-analyzed the HIP data and placed an upper mass limit on both planets c and d of $8.3 M_{Jup}$ and $14.2 M_{Jup}$, but did not claim true masses.

v And became the first multi-planet system to have a positive astrometry detection above 3σ when McArthur et al. (2010) detected the orbits of planets c and d using *Hubble Space Telescope* (*HST*). Their orbital fit included all previously obtained RVs (including re-reduced Lick data), and added RVs from the Hobby-Eberly Telescope at McDonald Observatory. The combined astrometry+RV fit did not converge when planet b was included, indicating that planet b presents no astrometric signal. Indeed, using their Equation 8, which relates the RV and astrometry, planet b would be expected to have a signal of $\alpha \sim 40 \mu\text{as}$ at an inclination of $\sim 3^\circ$, well below *HST*’s detection limit of 0.25 mas. This non-detection puts a weak upper mass limit on planet b of $\sim 78 M_{Jup}$, as the planet would be astrometrically detectable by *HST* at inclinations below $\sim 0.5^\circ$.

McArthur et al. (2010) found that planets c and d have inclinations of $7.868^\circ \pm 1.003^\circ$ and $23.758^\circ \pm 1.316^\circ$, respectively, relative to the plane of the sky, with corresponding masses of $13.98_{-5.3}^{+2.3} M_{Jup}$ and $10.25_{-3.3}^{+0.7} M_{Jup}$. The mutual inclination between the two planets is $29.917^\circ \pm 1^\circ$. This value is quite unlike any mutual inclination found amongst the planets of our Solar System. Subsequent dynamical studies suggest that this may be the result of a three-body planet-planet scattering scenario in which one planet is ejected from the system (Barnes et al. 2011; Libert & Tsiganis 2011).

By looking at the infrared excess in the stellar spectrum attributed to planet b, Harrington et al. (2006) attempted to chart the phase offset, i.e. the angle between the hottest point on the surface and the sub-stellar point. Assuming a radius of $< 1.4 R_{Jup}$, the observed amplitude of flux variation demanded that the planet’s inclination must be $> 30^\circ$ from the plane of the sky. Unfortunately, this study was based on only five epochs of data over a single orbit, and thus does not provide tight constraints.

The infrared phase curve of v And b was revisited with seven additional short epochs and one continuous ~ 28 hour observation by Crossfield et al. (2010). The picture presented in Crossfield et al. (2010) was consistent with Harrington et al. (2006), but they allowed larger radii in their model, finding that the inclination must be $> 28^\circ$ for a $1.3 R_{Jup}$ planet and $> 14^\circ$ for a $1.8 R_{Jup}$.

There is marginal evidence for a fourth planet orbiting v And. McArthur et al. (2010) found an improvement in their fit when a linear trend indicative of a longer period planet was included. Later, Curiel et al. (2011) found a signal at 3848.9 days using the Lick (Fischer et al. 2003; Wright et al. 2009) and ELODIE radial velocities (Naef et al. 2004). These authors have taken this to be a fourth planet in the system, as suggested by McArthur et al. (2010). The McArthur et al. (2010) analysis used re-reduced Lick data (received by personal communication from Debra Fischer) for their combined RV and astrometry orbital fit. As explained in McArthur et al. (2014, in press), these data include updated γ values (constant velocity offsets in the RVs) that removed this signal from the Lick data. Later, Tuomi et al. (2011) analyzed the older published RV data sets (Fischer et al. 2003; Wright et al. 2009) and also found a period for this fourth planet (that was an artifact of the missing γ) of 2860 days, but noted that the data sets seemed inconsistent. Tuomi et al. (2011) performed fits and calculated the Bayesian inadequacy criterion for the individual data sets. They found that the Wright et al. (2009) Lick data produced a significantly different period for planet e (3860 days) and the Bayesian inadequacy criterion indicates that this data set has a > 0.999 probability of being inconsistent with the other data sets. While a longer period planet, indicated by a small slope in the radial velocities, may exist in this system, the 4th planet signal reported by Curiel et al. (2011) was a product of the earlier reduction of the Lick data, which did not account for an instrument change that caused a shift in the γ . For this reason, we do not include this planet in our study.

The rotation and obliquity of v And A are also of interest in this study (see section 3.1). Measurements of $v \sin i = 9.6 \pm 0.5 \text{ km s}^{-1}$ (Valenti & Fischer 2005) and stellar radius $R_\star = 1.64_{-0.05}^{+0.04} R_\odot$ (Takeda et al. 2007) limit the rotation period to be $\lesssim 8$ days for physical values of i , however the only measured period consistent with these data is 7.3 days (Simpson et al. 2010). This period suggests an obliquity $i \sim 60^\circ$ (measured from the sky plane), but the signal at this period is very weak and it is impossible to distinguish this obliquity from $i \sim 120^\circ$ (spinning in the opposite sense).

1.2 Theory

Numerous dynamical studies of v Andromedae have been performed, both numerical and analytical. Early studies focused on the stability of the system using N-body models and analytic theory, prior to the astrometric detection of planets c and d (McArthur et al. 2010). These studies showed that the stability of the system is highly sensitive to the eccentricities of planets (d in particular) (Laughlin & Adams 1999; Barnes & Quinn 2001, 2004), the relative inclinations of the planets (Rivera & Lissauer 2000; Stepinski et al. 2000; Chiang et al. 2001; Lissauer & Rivera 2001; Ford et al. 2005;

Michtchenko et al. 2006), their true masses (since only minimum masses were known prior to McArthur et al. 2010) (Rivera & Lissauer 2000; Stepinski et al. 2000; Ito & Miyama 2001), the effect of general relativity on planet b’s eccentricity (Nagasawa & Lin 2005; Adams & Laughlin 2006; Migaszewski & Goździewski 2009), and the accuracy of the RV data (Lissauer 1999; Stepinski et al. 2000; Goździewski et al. 2001), and also found that there were stable regions only between planets b and c and exterior to planet d (Rivera & Lissauer 2000; Lissauer & Rivera 2001; Barnes & Raymond 2004; Rivera & Haghighipour 2007). The dynamical study of McArthur et al. (2010) found stable configurations for all three planets on a timescale of 10^5 years, and constrained the inclination of planet b to $i < 60^\circ$ or $i > 135^\circ$. It has also been demonstrated that analytical or semi-analytical theory does not adequately describe the dynamics of the system (Veras & Armitage 2007), unless taken to very high order in the eccentricities (Libert & Henrard 2007), though these studies assumed coplanarity since the inclinations of the planets were not known at the time.

Other studies dealt with the evolution and formation of certain features of the system, in particular the apparent alignment of the pericenters (or “apsidal alignment”, $\Delta\varpi$, noted by Rivera & Lissauer (2000); Chiang et al. (2001)) and large eccentricities of planets c and d. Some have investigated whether the present day system could have been produced by interactions with a dissipating disk (Chiang & Murray 2002; Nagasawa et al. 2003), by planet-planet scattering (Nagasawa et al. 2003; Ford et al. 2005; Barnes & Greenberg 2007a; Ford & Rasio 2008; Barnes et al. 2011), by interactions with the stellar companion, ν And B (Barnes et al. 2011), by secular or resonant orbital evolution (Jiang & Ip 2001; Malhotra 2002; Ford & Rasio 2008; Libert & Tsiganis 2011), or by accelerations acting on the host star (Namouni 2005). Michtchenko & Malhotra (2004) found that $\Delta\varpi$ can be in a state of circulation, libration or a “non-linear secular resonance”, all within the observational uncertainty. In short, the dynamical evolution of the system appears to be highly sensitive to the initial conditions, and planet-planet scattering appears to be the most promising explanation for its current state.

In particular, McArthur et al. (2010) noted that the true masses of planets c and d naturally resolve a difficulty in explaining the system’s formation. When only the minimum masses of the two planets were known, it was generally assumed in dynamical analysis that planet d was the larger ($m \sin i_c = 1.8898 M_{Jup}$ and $m \sin i_d = 4.1754 M_{Jup}$), however, mechanisms that can excite the eccentricities of the planets, such as resonance crossing (Chiang et al. 2002) or close encounters (Ford et al. 2001), tend to result in the smaller mass planet having the larger eccentricity. Some authors noted that because planet d is observed to have the larger eccentricity ($e_c = 0.245 \pm 0.006$, $e_d = 0.316 \pm 0.006$ (McArthur et al. 2010)), the formation of the system may have required the presence of a gas disk or the ejection of an additional low-mass planet (Chiang et al. 2002; Rivera & Lissauer 2000; Ford et al. 2005; Barnes & Greenberg 2007b).

Finally, Burrows et al. (2008) produced theoretical pressure-temperature profiles and spectra for several

close-in giant planets, including ν And b, and compared these results with the phase curve in Harrington et al. (2006). Unfortunately, the phase curve data were too sparse to make any conclusions about the size or structure of the atmosphere or the planet’s inclination, only that a range of radii and inclinations are consistent with the data, and that a temperature inversion in the atmosphere is also consistent. The authors suggested that more frequent observations and multi-wavelength data may break the degeneracies in their model.

1.3 This Work

Observations account for the inclinations and true masses of planets c and d, but the inclination and true mass of planet b remain undetermined. Early dynamical studies found stable regions of parameter space for the coplanar, three planet system, however, stable configurations have not previously been identified for three planets over long timescales since the large mutual inclination between planets c and d was discovered by astrometry. Additionally, it is unclear whether the phase curve observations (Harrington et al. 2006; Crossfield et al. 2010) are consistent with the RV+astrometry observations (McArthur et al. 2010). Here we explore all the above issues using dynamical models.

This work is a sweep through parameter space for stable configurations for all three planets, following up on the dynamical analysis in McArthur et al. (2010). An acceptable configuration in this study is one that 1) satisfies the RV+astrometry fit (McArthur et al. 2010), 2) is dynamically stable, and 3) is consistent with the IR phase curve measurements (Crossfield et al. 2010). Our results satisfy all three criteria, however, reconciliation with the phase curve measurements requires planet b to have an inflated radius and motivates us to include tidal heating in this study.

Section 2 describes the methods that we use to explore parameter space, model the dynamics, and estimate tidal heating in planet b. Section 3 describes the results we obtain for stability and system evolution. Section 4 focuses on tidal heating and reconciliation with Crossfield et al. (2010). In Section 5, we discuss our results in the context of previous studies, and summarize our conclusions in Section 6.

2 METHODS

2.1 Updated Orbits and Parameter Space

As in McArthur et al. (2010), all RV data sets are re-examined using the published errors (which are large for the AFOE data, in particular). The Lick data set has been re-reduced since the original publications, resulting in new γ offsets. This updated set, published recently in Fischer et al. (2014), was used in McArthur et al. (2010) (received by personal correspondence with D. Fischer), and similarly we use it here. The RV fit is performed on each data set individually and compared with the other data sets for consistency, and large outliers are examined and removed, if necessary.

Trials are generated by drawing randomly from within the uncertainties of the χ^2 best fit to the RV and astrometric data. Table 1 shows the parameter space explored. The astrometric constraints on the semi-major

axes of planets c and d are ignored as the RV derived periods provide much stricter constraints on these quantities. Trials are not generated taking into account interdependencies of the various parameters, however, because of the small size of the uncertainties all trials should be faithful to the data. Nevertheless, we include χ^2 values for our stable cases to confirm consistency. This work is not meant to represent a complete analysis of all possible configurations. We are merely establishing the existence of stable cases within the observational constraints

The nominal eccentricity of planet d is 0.316, however, we find that very few trials are stable above $e_d \sim 0.3$ (see Figure 1), so we apply a much looser constraint to the lower bound of planet d’s eccentricity, drawing from a uniform distribution across the domain $0.246 < e_d < 0.322$, rather than a Gaussian distribution.

2.2 N-Body

For the stability analysis, we use *HNBody* (Rauch & Hamilton 2002), which contains a symplectic integrator for central-body-like systems, i.e., systems in which the total mass is dominated by a single object. This symplectic scheme alternates between Keplerian motion and Newtonian perturbations at each timestep (see Wisdom & Holman 1991). During one half-step (the “kick” step), all gravitational interactions are calculated and the momenta are updated accordingly. During the other half-step (the “drift” step), the system is advanced along Keplerian (2-body) motion, using Gauss’s f and g equations (see Danby 1988). The entire integration is done in Cartesian coordinates. Unlike *Mercury* (Chambers 1999), post-Newtonian (general relativistic) corrections are included as an optional parameter in *HNBody*, and we utilize them here.

While *HNBody* is fast and its results compare well with results from *Mercury*, its definitions of the osculating elements used at input and output differ slightly from *Mercury*’s. The mass factor used in the definitions of semi-major axis and eccentricity (for astrometric or barycentric elements) does not include the planet’s mass; in other words, the planet is treated as a zero mass particle during input and output conversions between Cartesian coordinates and osculating elements. Because of this, the use of osculating elements during input can result in incorrect periods and Cartesian velocities. For most planetary systems, which have poorer constraints on the periods and semi-major axes of the planets, this aspect makes little difference, but for ν Andromedae the periods are known with the high precision that comes with > 15 years of RVs, and so all of our input and output from *HNBody* is done in Cartesian positions and velocities, to ensure proper orbital frequencies.

A second important conversion must be done to account for a difference in units. *HNBody* and *Mercury* enforce the relationship $GM_\odot D^2/au^3 = k^2$, where k is the Gaussian gravitational constant (defined to be $0.01720209895 \text{ au}^{3/2} M_\odot^{-1/2} D^{-1}$), D is the length of the day, and au is the astronomical unit, based on the IAU definitions prior to 2012. The current accepted IAU units fix the au to be exactly 149,597,870,700 m and the constant k is no longer taken to be a constant value. This redefinition was done for ease of use and to allow for reconciliation with the length-contraction and time-dilation

of Einstein’s relativity. Because these N-body models were developed prior to this redefinition, k was used as a fundamental constant, as that allowed for better accuracy in Solar System integrations when the au was uncertain. We believe these integrators still accurately represent the dynamics of planetary systems, since these models do not attempt to account for length-contraction and time-dilation and in any case these effects will be very small. Note that *HNBody* does account for relativistic precession, which is important for the motion of planet b, as mentioned in Section 1.2.

The units utilized by the integrator are then au, days, and solar masses. For observations of exoplanets, SI units are more sensible, but the values of G , M_\odot , and au need not obey the above constraint. Hence the simulated orbital periods will not be equal to the measured orbital periods unless we first convert from SI units, which do not obey this constraint, to IAU units, which do. We accomplish this by choosing a value for the au which satisfies $GM_\odot D^2/au^3 = k^2$, given the G , M_\odot , and D used in the model of the observations. We then check that this definition of the au correctly reproduces the orbital periods of the planets when calculated using k and Kepler’s third law,

$$T^2 = \frac{4\pi^2}{k^2(M_\star + m_p)} a^3, \quad (1)$$

where T is the planet’s period in days, M_\star and m_p are the masses of the star and planet in solar masses, and a is the planet’s semi-major axis in au. Finally, to verify that *HNBody* “sees” the correct periods, we run 2-body integrations for each planet at high time resolution and performed FFTs on the planets’ velocities, confirming that this approach is the most accurate.

For the reasons described above, we take the orbital elements from the RV+astrometry, convert to Cartesian coordinates for dynamical modelling, then convert back to orbital elements for stability analysis. For analysis of the orbital evolution, we convert from Cartesian “line-of-sight” coordinates to Cartesian invariable plane (the plane perpendicular to the total angular momentum of the system) coordinates prior to the conversion back to orbital elements. The invariable plane of the system is inclined by $\sim 15^\circ$ from the sky, so inclinations measured from this plane are similar to those measured from the sky-plane. See the appendix for a potential pitfall in modelling astrometrically measured orbits.

The initial parameter space includes inclinations of planet b from 0° to 180° , which is to say that any inclination is consistent with the observations. Extremely low inclination, $i_b < 1^\circ$ or $i_b > 179^\circ$, places the mass of planet b in the brown dwarf range. Inclinations $\gtrsim 90^\circ$ are retrograde orbits with respect to the orbits of the outer two planets (note that the outer system’s invariable plane is inclined only $\sim 10^\circ$ from the sky plane). The observations allow for such configurations, and we cannot rule them out based on dynamical stability.

2.3 Tidal Theory

We use a constant phase-lag (CPL) model (Darwin 1880) to estimate the amount of tidal energy that could be dissipated in the interior of ν And b. This model is described in detail in appendix E of Barnes et al. (2013)

TABLE 1

Parameter space: PARAMETERS ARE DRAWN FROM GAUSSIAN DISTRIBUTION WITH CENTER (STANDARD DEVIATION) EXCEPT WHERE NOTED

	v And b	v And c	v And d
e	0.01186 (0.006)	0.2445 (0.1)	0.316 (0.07/0.006)*
i ($^\circ$)	90 (90) [†]	11.347 (3.0)	25.609 (3.0)
ω ($^\circ$)	44.519 (24.0)	247.629 (2.2)	252.991 (1.32)
Ω ($^\circ$)	180 (180) [†]	248.181 (8.5)	11.425 (3.31)
P (days)	4.61711 (0.00018)	240.937 (0.06)	1281.439 (2.0)
T (days)	2450034.058 (0.3)	2449922.548 (1.5)	2450059.072 (4.32)
K (m/s)	70.519 (0.368)	53.4980 (0.55)	67.70 (0.55)

*drawn from a uniform distribution with lower/upper bounds shown

[†]uniform distribution

(see also Ferraz-Mello et al. 2008). In short, the model treats the tidal distortion of the planet as a superposition of spherical harmonics with different frequencies, which sum to create a tidal bulge that lags the rotation by a constant phase. The strength of tidal effects is contained in the parameter Q , called the tidal quality factor, estimated to be $\gtrsim 10^4$ for the planet Jupiter (Goldreich & Soter 1966; Yoder & Peale 1981; Aksnes & Franklin 2001). For close in Jovians like v And b, Ogilvie & Lin (2004) suggest Q could be as high as 5×10^7 , hence we model a range of Q values from $10^4 - 10^8$.

The CPL model, commonly used in the planetary science community, is only an approximate representation of tidal evolution (for an in-depth discussion of the limitations of the model, see Efroimsky & Makarov 2013). However, at the eccentricities we explore here ($e \lesssim 0.15$), results from this model are qualitatively similar to other tidal models. The CPL model has the advantage of fast computation and is accurate enough for our purpose here, which is merely to establish the possibility of tidal heating in the interior of planet b. Given the uncertainty in the model and in the properties of the planet, our results should not be taken to be a precise calculation of the planet’s tidal conditions.

3 ORBITAL DYNAMICS

In this section, we present our results regarding the dynamics of the system. In Section 3.1, we examine the stability of the system. In Section 3.2, we compare the orbital evolution in our favored cases.

3.1 Stability

We run our initial set of 1,000 trials for 1 Myr and flag as unstable those trials in which one or more planets were lost. The resulting stability maps are shown in Figure 1. Here we show the most relevant parameters, i.e., those with the largest uncertainty (Ω_b and i_b) and those which have a large effect on stability (e_c and e_d). The coordinate system used here is the RV+astrometry (“line-of-sight”) coordinate system, in which i is measured from the plane of the sky and Ω is measured counterclockwise from North.

We note regions of greater stability concentrate around inclinations for planet b of $\lesssim 40^\circ$ and $\gtrsim 140^\circ$ and ascending nodes of $\sim 0^\circ$. A chasm of instability lies across inclinations of $\sim 60^\circ$ to $\sim 140^\circ$.

Next we examine the eccentricity and inclination evolutions for all trials in which three planets survived 1 Myr. Many of these “stable” cases exhibit chaotic evolution,

with planet b even reaching eccentricities of ~ 0.9 . We assume trials with chaotic evolution are in the process of destabilizing and should be discarded. This leaves us with ~ 30 trials which we then ran for 100 Myrs. Trials in which all planets survive 100 Myr integrations with no chaotic evolution or systematic regime changes are considered robustly stable. These 10 cases are plotted as x’s in Figure 1.

v Andromedae is estimated to be ~ 3 Gyrs old (Takeda et al. 2007); our ideal goal would thus be to demonstrate stability over this timespan; however, because a very small timestep is necessary to resolve the 4.6 day orbit of planet b, simulations of the system on spans of Gyrs are computationally prohibitive. Hence, we limit ourselves to a domain of 100 Myrs (1/30th of the system’s lifetime), and note that this length of time corresponds to ~ 8 billion orbits of planet b and that no previous study has been able to show stability for all three planets on this timescale.

The χ^2 results for our stable cases are shown in Table 2. Here, χ^2 represents the goodness of fit of each configuration to the data, and would ideally be equal to the number of degrees of freedom (DOF) in the model of the data. Configuration **PRO1** is chosen as our nominal case because it has the lowest χ^2 value of the prograde (orbit of planet b) cases.

For our 4 prograde, stable trials, we generate the stability maps shown in Figure 2. Keeping all other parameters constant, we vary the inclination and ascending node of planet b to further explore these “islands” of stability. In order to keep all our cases consistent with the observations of planet b, we adjust its mass with changes in inclination and subsequently must adjust its semi-major axis to maintain the observed period. Thus changes in inclination imply not only a different mass via the $m \sin i$ degeneracy, but also a change in semi-major axis.

In all cases we see that our solutions occupy stable regions of phase space. **PRO2** and **PRO3** appear to be perched on the edges of two large stable regions, while **PRO1** occupies a very narrow stable “inclination stripe” at $\sim 5^\circ$ and $\sim 2 - 3^\circ$, respectively. As in Figure 1, inclination in Figure 2 is measured from the sky-plane, not the invariable plane of the system.

An additional complication to the dynamics of the system is the oblateness of the host star. Migaszewski & Goździewski (2009) showed the importance of J_2 (the leading term in the gravitational quadrupole moment) of the star in their secular analysis, though they used a stellar radius of $R = 1.26 R_\odot$, significantly smaller than the current best measurement of $R = 1.631 \pm 0.014 R_\odot$

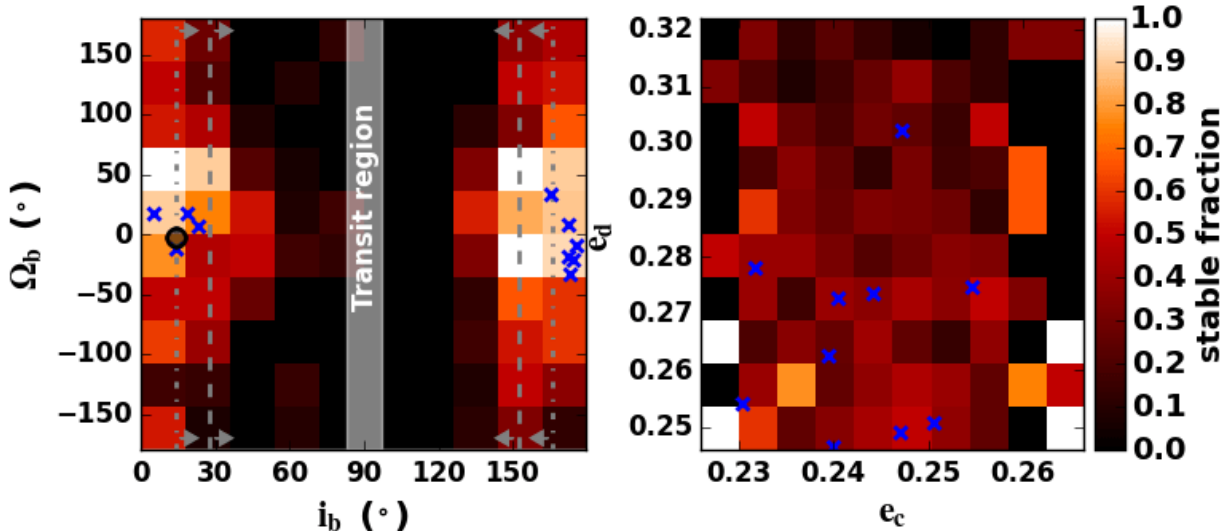


FIG. 1.— Stable fraction ($f_s = N_s/N$, where N_s is the number of trials that survived 1 Myr in each bin and N is the total number of trials in each bin), for different parameters. Left: Longitude of ascending node (Ω_b) vs. inclination (i_b) of planet b. The x 's represent our robustly stable cases that survived for 100 Myr with no signs of chaos. The black circle represents the average fundamental plane of a system with planets c and d only. Shown also are the inclinations predicted by Crossfield et al. (2010) (dashed line: $R_p > 1.3R_{Jup}$; dotted line: $R_p > 1.8R_{Jup}$) and the region for which the planet would transit the host star. Higher stability occurs at $i_b \lesssim 40^\circ$ and $i_b \gtrsim 140^\circ$. Right: Eccentricity of planet d vs. eccentricity of planet c. Stability is most dependent on e_d , which must remain $\lesssim 0.3$ for the system to remain stable. Stability seems uncorrelated with e_c (the bright colored bins on the far left and far right contain only 1-2 trials each, and are therefore not necessarily regions of high stability).

TABLE 2
Stable configurations

Trial	χ^2 (DOF = 811)
PRO1	779
PRO2	2218
PRO3	2353
PRO4	3378
RETRO1	672
RETRO2	725
RETRO3	1292
RETRO4	1524
RETRO5	1917
RETRO6	3062

(Baines et al. 2008). To verify the importance of oblateness, we simulated our best prograde χ^2 case (**PRO1**), varying J_2 from 10^{-5} to 10^{-2} and R_* from $1.26 R_\odot$ to $1.63 R_\odot$. We find that values of $J_2 \gtrsim 10^{-3}$ cause the system to become unstable, and lower values significantly change the eccentricity evolution of planet b. Unfortunately, the J_2 value of the star is not known and there exists some disagreement regarding its radius, and thus a detailed exploration of parameter space including these two additional parameters is beyond the scope of this work. Therefore, in our primary analysis, the quadrupole moment is ignored ($J_2 = 0$).

3.2 System Evolution

The eccentricity and inclination evolutions for our prograde trials are shown in Figures 3 - 6. In these figures, inclination is measured from the invariable plane, that is, a plane perpendicular to the total angular momentum vector of the system. We see that for all cases, the evolution of the eccentricities and inclinations is periodic for at least 100 Myrs (~ 8 billion orbits of planet b). At a glance, one might expect for **PRO1** to lose planet

b, however, as shown in Figure 3, the pattern seen in its eccentricity evolution is repeated reliably over many orbits, and therefore the configuration is robustly stable.

For planets c and d, Figures 7 and 8 show $\Delta\varpi = \varpi_d - \varpi_c$ (the difference of the longitudes of pericenter) and their mutual inclination Ψ_{cd} for our cases in which planet b is in prograde motion. We see that $\Delta\varpi$ undergoes circulation in cases **PRO1** and **PRO2**, and librates around anti-alignment in cases **PRO3** and **PRO4**, although it is very close to the separatrix in both. The amplitudes of libration are $\sim 240^\circ$ and $\sim 210^\circ$, for **PRO3** and **PRO4**, respectively, and RMS values about the libration center (180°) are 55° and 47° , respectively. The mutual inclination between planets c and d oscillates between $\sim 30^\circ$ and $\sim 40^\circ$ in cases **PRO2**, **PRO3**, and **PRO4**. The angle explores a slightly wider range in case **PRO1**.

4 TIDAL HEATING

The phase curve measurements (Crossfield et al. 2010) require planet b to have a radius of $1.3 R_{Jup}$ at an inclination of 28° ($1.8 R_{Jup}$ at $i = 14^\circ$). This large radius could be explained by a combination of intense stellar irradiation and tidal heating in the planet's interior. To that end, we present predictions of tidal energy dissipation in several of our cases.

In reference to the planet HD 209458 b, Ibgui & Burrows (2009) found that early episodes of high eccentricity can cause tidal dissipation of $\sim 10^{19}$ watts of power, which helps to explain the planet's radius of $1.3 R_{Jup}$, though it may not be necessary, considering the stellar flux received. We find that planet b in our prograde cases experiences significant eccentricity evolution (Figures 3 - 6), which should trigger similar episodes of tidal heating. As discussed in section 5, this may be necessary to

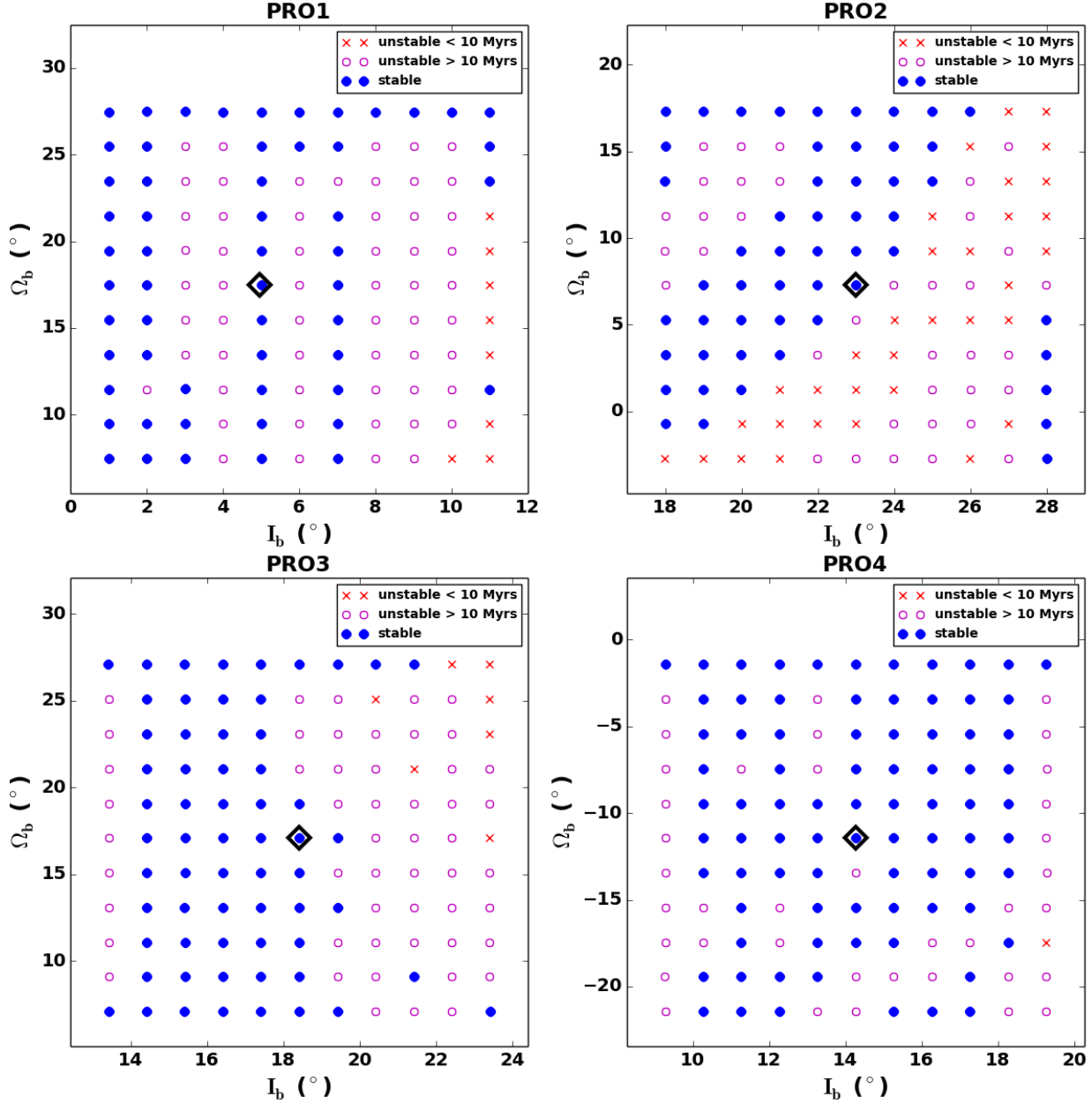


FIG. 2.— Stable regions surrounding our prograde trials, varying the orbital plane of planet b. Red x 's are trials that had a planet ejected in less than 10 Myrs, pink circles displayed chaotic evolution but no ejections over 10 Myrs, and blue solid circles are those which are truly stable over 10 Myrs. The original trials are surrounded by the black diamonds.

reconcile our results with that of Crossfield et al. (2010).

In Figure 9 we show tidal energy dissipated in the interior of planet b for case **PRO1**. Tidal heating for **PRO2** looks very similar. We explore a range of tidal factor Q (left panel, with planet radius $R = 1.5 R_{Jup}$) and planet radius (right panel, with $Q = 10^6$). We find that, depending on the true radius of the planet and the equation of state of the interior, planet b could indeed have episodes of intense tidal heating. Coupled with the intense stellar radiation at ~ 0.06 au, for the case **PRO2**, this could reconcile the results of McArthur et al. (2010), Crossfield et al. (2010), and this study (see the right panel in Figure 9).

The results are more difficult to reconcile for the lower inclination case **PRO1**. Miller et al. (2009) showed that

radius inflation for hot Jupiters is a strong function of mass. Referring to their Figure 6, with $10^{19} \text{ W} = 10^{26} \text{ erg s}^{-1}$, and the mass of planet b of $\sim 8 M_{Jup}$ for **PRO1**, it seems unlikely that even the combination of tidal heating and stellar irradiation could inflate planet b beyond $\sim 1.5 R_{Jup}$. Additionally, the planet in that case would need to have a radius of $> 3 R_{Jup}$ in order to explain the phase curve. However, given the lingering uncertainty in the apparently large radii of some hot Jupiters, as well as the shortcomings of tidal theory, these configurations may still be compatible with the Crossfield et al. (2010) results.

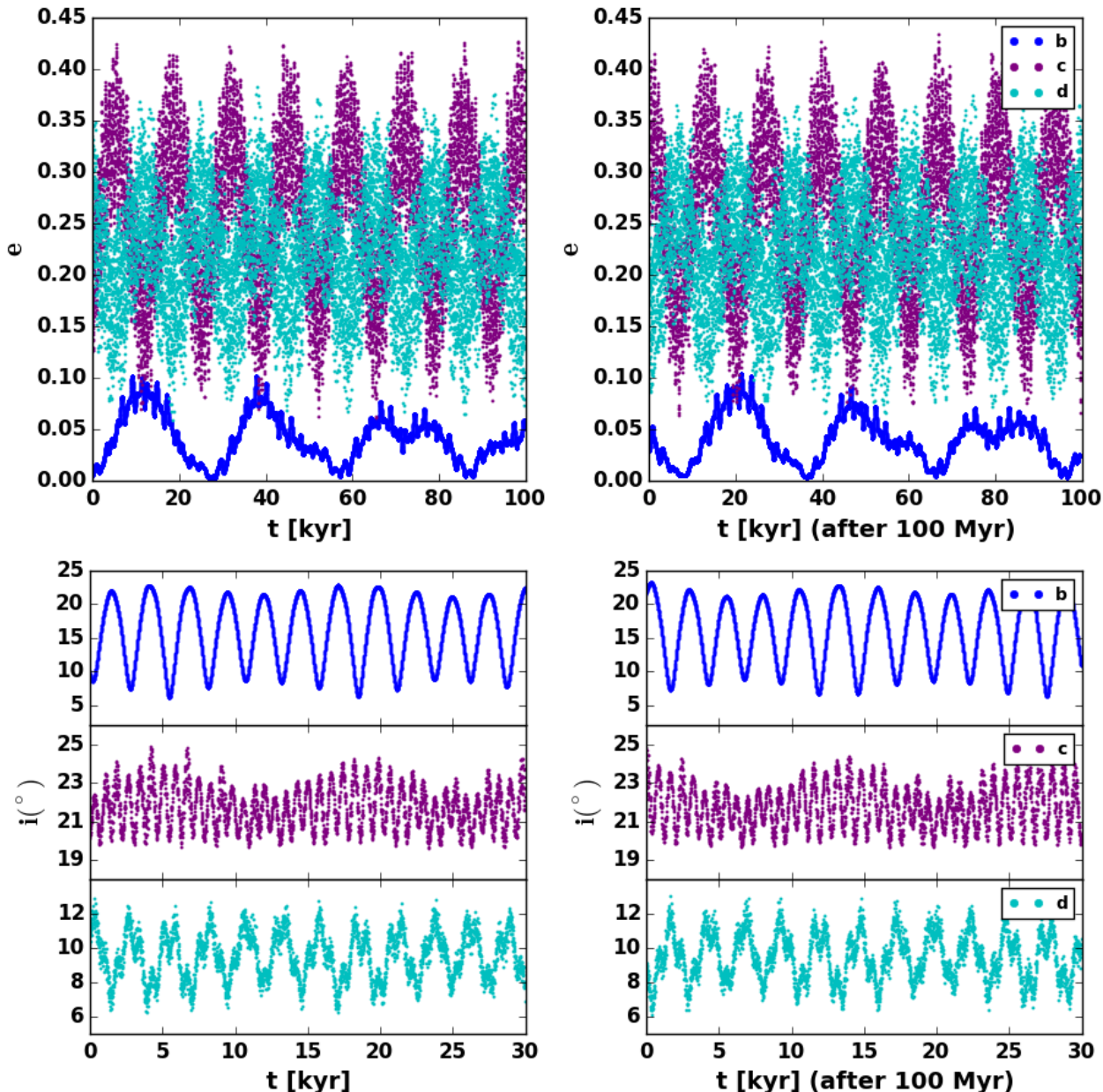


FIG. 3.— Eccentricity evolution (top panels) and inclination evolution (bottom panels) for planet b (blue), planet c (purple), and planet d (cyan) over 100,000 years, from the current epoch (left) and after a 100 Myr integration (right), in the **PRO1** system. The eccentricity evolution of planet b may appear unstable, but as seen in the right panel, the pattern is periodic over at least 100 Myr timescales. Inclinations here are measured from the invariable plane of the system, rather than the sky-plane.

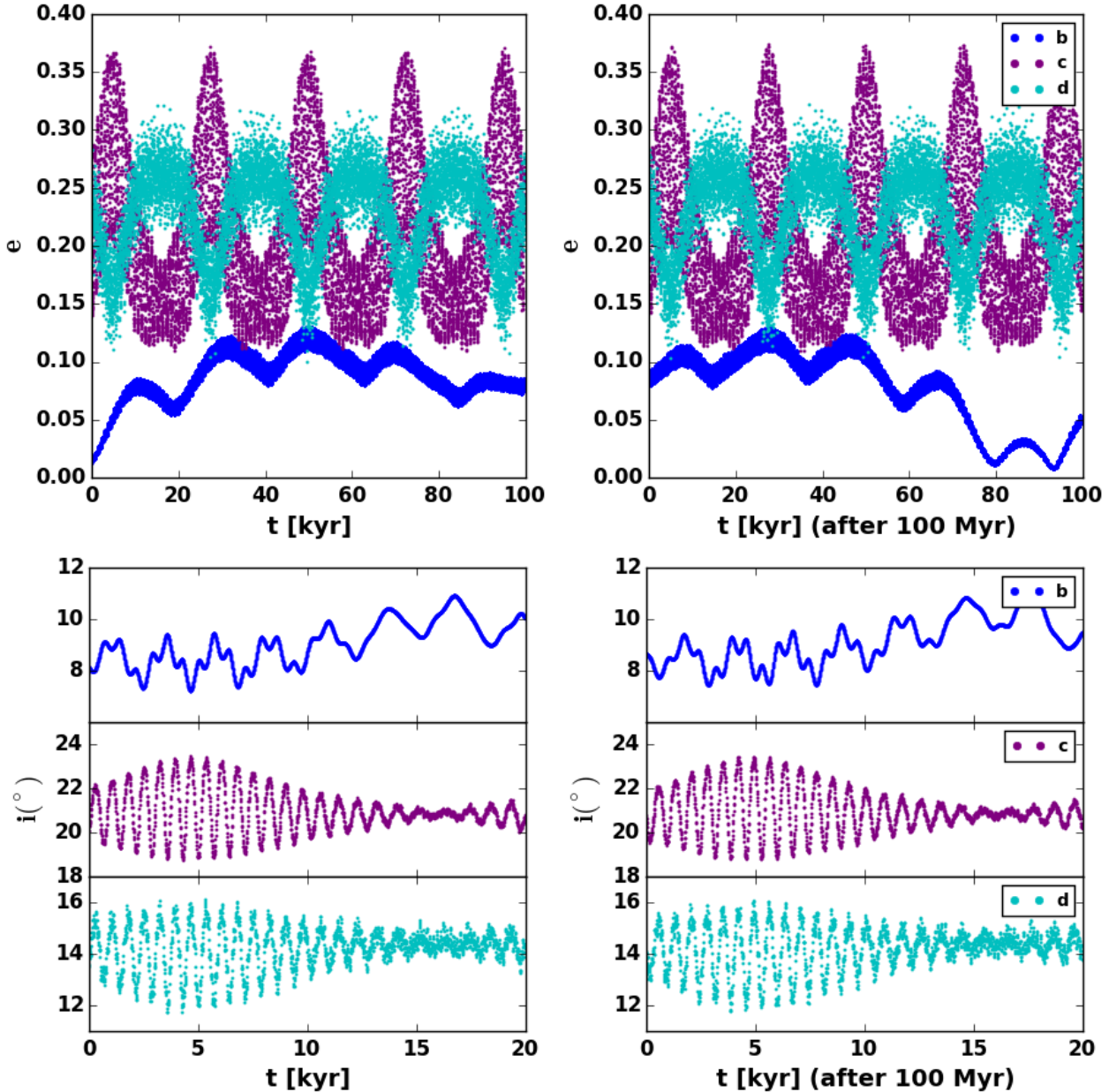
5 DISCUSSION

Only four of our stable architectures (three of them prograde) are fully consistent with Crossfield et al. (2010), which requires that planet b in these cases be as large as $1.8 R_{Jup}$, and would place it amongst the largest known exoplanets. Still, this size is reasonable, as, for example, the radius of the hot Jupiter HAT-P-32 b was determined to be $R = 2.037 \pm 0.099 R_{Jup}$ —a planet orbiting a star of similar spectral type (late FV) and age (~ 3 Gyr) to v And (Hartman et al. 2011). We have demonstrated that the eccentricity evolution of planet b in several cases allows for significant tidal energy dissipation which will help to explain its very large size.

Yet the case with the lowest χ^2 value, **PRO1**, has an

inclination of $\sim 5^\circ$ for planet b, which may be more difficult to reconcile with the Crossfield et al. (2010) result. From Equation 2 in Crossfield et al. (2010), we conclude that planet b in **PRO1** would have to have a radius of $\sim 3 R_{Jup}$ to be consistent with the phase curve measurements, while its large mass may prevent inflation to even beyond $\sim 1.5 R_{Jup}$.

There are two retrograde cases with comparable χ^2 to our nominal solution, but we cautiously favor prograde orbits for planet b over retrograde on the grounds that it is difficult to explain the formation of a multi-planet system with mutual inclinations this extreme ($\Psi \sim 180^\circ$). Transits of many hot Jupiters have permitted detection of a Rossiter-McLaughlin effect, in which the alignment

FIG. 4.— As in Figure 3 but for case **PRO2**

of the planet’s orbit, relative to the spin axis of the star, can be inferred from asymmetries during the transit in Doppler-broadening spectral lines (Triaud et al. 2010). A significant number of these orbits are misaligned with the stellar obliquity, however, as ν And A’s obliquity is unknown, it is impossible to say at this time whether our so-called “retrograde” orbits are in fact misaligned with the star’s rotation (or that our prograde orbit are aligned with it). Rather, it is the high mutual inclination between planet b and planets c and d that must be explained in order to justify our retrograde cases. It is noteworthy that no detected exoplanet (and host star) with $> 90^\circ$ misalignment has been found in a multiple planet system. Because of the lack of observational precedent, we are reluctant to favor our retrograde systems.

Early studies found that the pericenters of planets c and d were oscillating about alignment, such that $\Delta\varpi =$

$\varpi_d - \varpi_c \sim 0^\circ$ (Chiang et al. 2001, 2002). Michtchenko & Malhotra (2004) found that $\Delta\varpi$ could take on a full range of behaviors from libration to circulation, based on initial conditions within the uncertainties of the observations at the time. Ford et al. (2005) found $\Delta\varpi$ near separatrix, and more recently, Barnes et al. (2011) found $\Delta\varpi$ librating about anti-alignment ($\Delta\varpi \sim 180^\circ$). Here, we have in our prograde cases a variety of behavior for $\Delta\varpi$: precession in one case, recession in two, and libration in two.

The exact nature of the secular relationship between planets c and d appears to be highly sensitive to the orbital parameters, as we see that $\Delta\varpi$ and Ψ_{cd} take on very different modes of behavior just within the observational uncertainties. It seems that the planets are close to an apsidal separatrix.

Whereas the orbital fit (McArthur et al. 2010) sug-

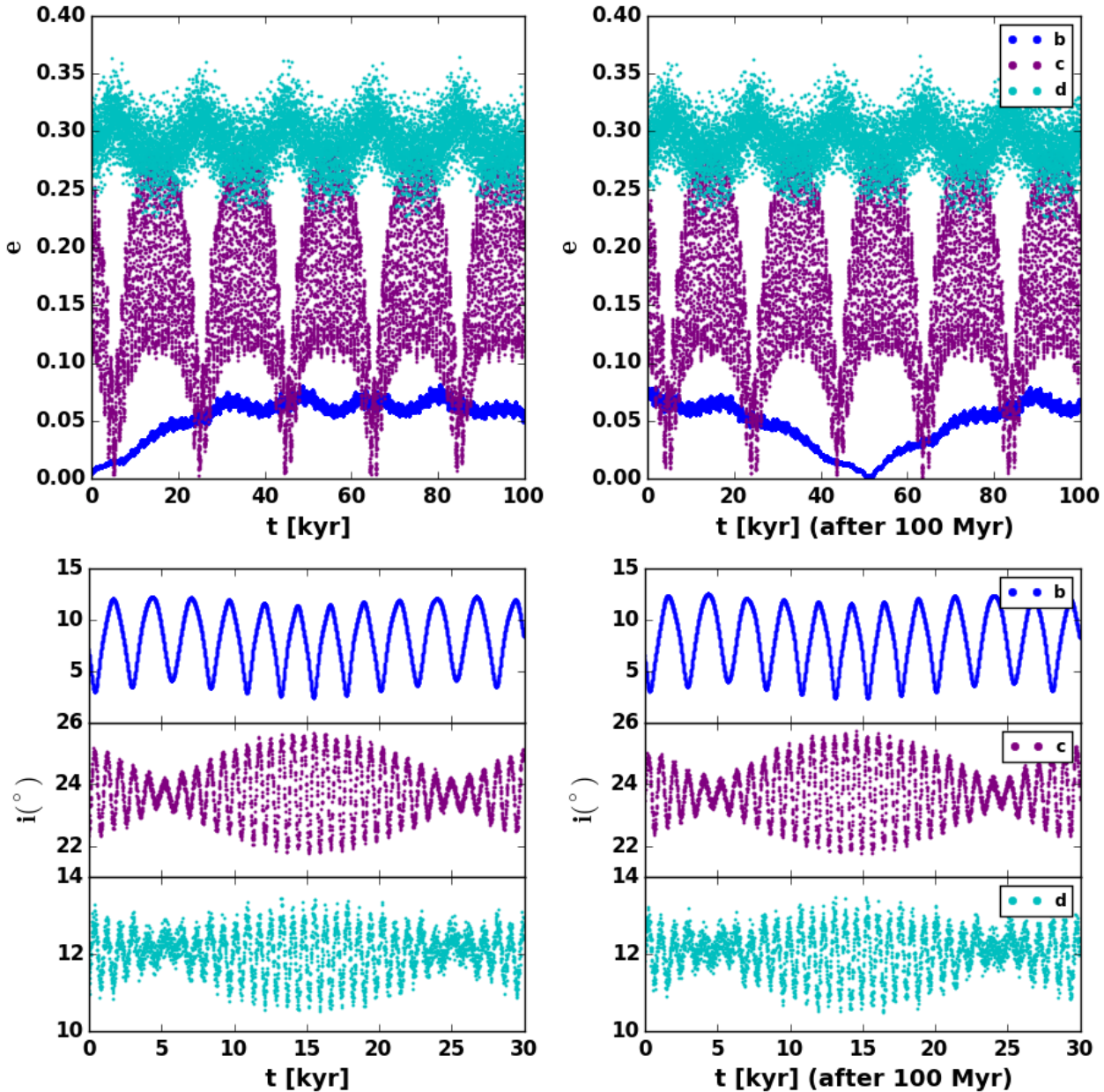


FIG. 5.— As in Figure 3 but for case **PRO3**

gests that planet c has larger mass than planet d, stability seems to slightly favor planet d having the larger mass (prograde cases only), though strong conclusions should not be drawn from only four examples. While this eccentricity ratio is less likely, Barnes et al. (2011) have shown that the relative inclinations are significantly more difficult to produce, and that planet-planet scattering resulting in the ejection of an additional planet is able to produce both features.

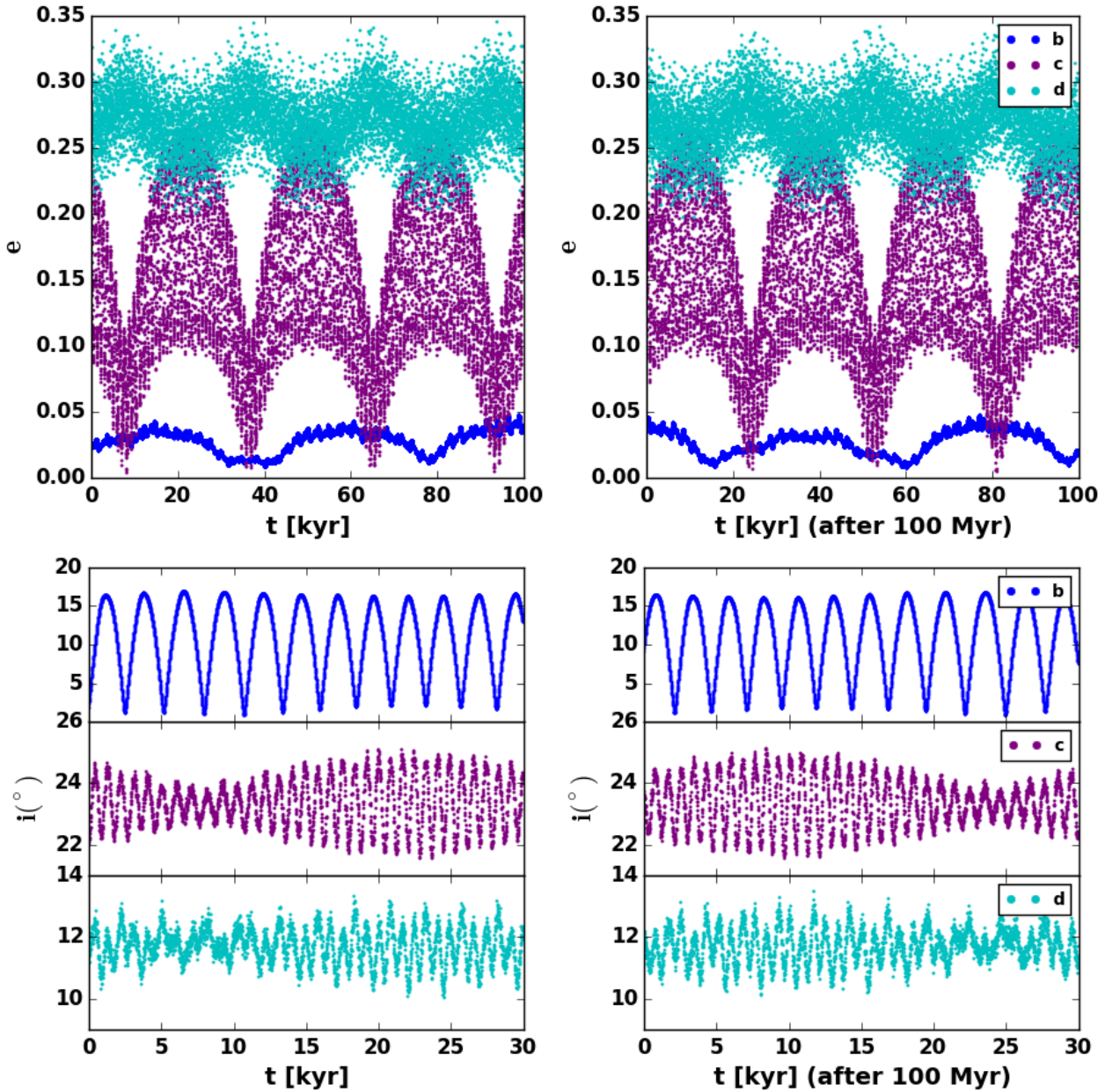
From Figure 2, it is clear that the system resides close to instability. This proximity to instability and the large eccentricities and mutual inclination of planets c and d suggest that the system arrived at its current configuration by a past planet-planet scattering event, as found by Barnes et al. (2011). The near-separatrix behavior of c and d additionally suggest that this event was more likely to be a collision than the ejection of a fourth planet

from the system (Barnes et al. 2011).

6 CONCLUSIONS

We have presented 10 dynamically stable configurations consistent with the combined radial velocity/astrometry fit first presented in McArthur et al. (2010). In six of these cases, planet b orbits retrograde with respect to planets c and d. Because of the apparent difficulty in the formation of such a system, our analysis focuses instead on the four remaining prograde cases. The case **PRO1** represents our best estimate of the system's true configuration, because of its low χ^2 and the relative ease of explaining its formation.

In our stable prograde results, planet b's inclination spans the range of $3^\circ \lesssim i_b \lesssim 23^\circ$. The corresponding mass range is $1.78 M_{Jup} \leq m_b \leq 13.57 M_{Jup}$. Three

FIG. 6.— As in Figure 3 but for case **PRO4**

of the four prograde trials are consistent with the predicted inclination from the infrared phase curve results (Crossfield et al. 2010), but require a planet radius of $\sim 1.3 - 1.8 R_{Jup}$.

ν Andromedae is a benchmark that may portend a new class of planetary system, i.e., “dynamically hot” systems with high eccentricities and high mutual inclinations. Currently ν And is the only multi-planet system with astrometry measurements, but *Gaia* (Casertano et al. 2008) and perhaps a *NEAT*-like mission (Malbet et al. 2012) will discover if such architectures are common or rare. If ν And-like systems are common in the galaxy, we should even expect to find potentially habitable planets in dynamically complex environments.

drigo Luger acknowledge support from the NASA Astrobiology Virtual Planetary Laboratory lead team. Russell Deitrick also acknowledges support from the University of Washington GO-MAP fellowship. Rory Barnes acknowledges support from NSF grant AST-1108882. Support for HST ν And was provided by NASA through grants GO-09971, GO-10103, and GO-11210 from the Space Telescope Science Institute, which is operated by the Association of Universities for Research in Astronomy (AURA), Inc., under NASA contract NAS5-26555. We would additionally like to thank Jonathan Fortney, Mike Line, and Eric Agol for helpful discussions.

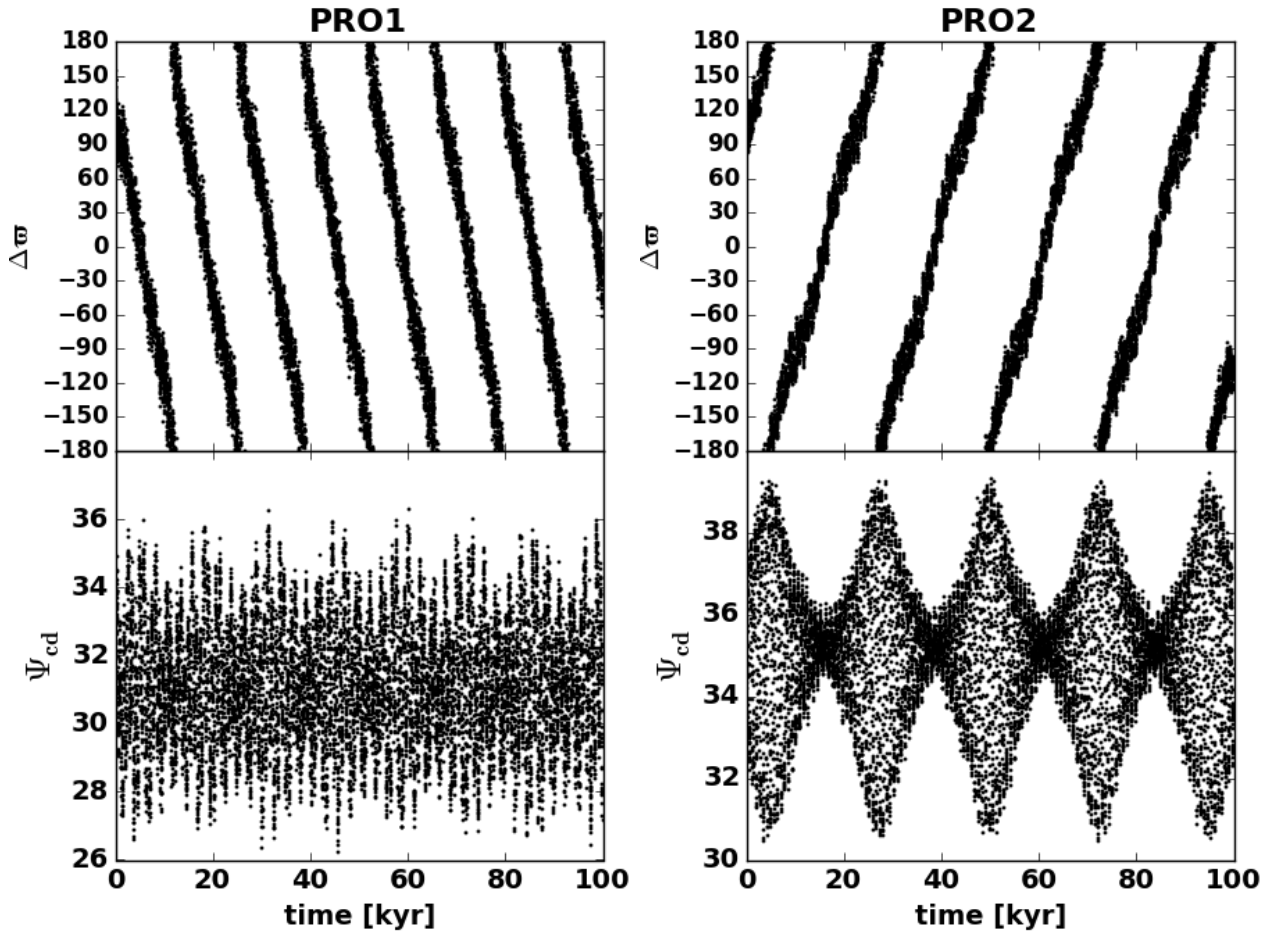


FIG. 7.— Secular behavior of planets c and d. $\Delta\varpi = \varpi_d - \varpi_c$ circulates in both cases. The mutual inclination, Ψ_{cd} , oscillates about $\sim 31^\circ$ in **PRO1** and $\sim 35^\circ$ in **PRO2** with a $\sim 10^\circ$ amplitude in both.

TABLE 3
Orbital parameters for stable, prograde trials

ID	planet	m (M_{Jup})	P (days)	a (au)	e	i ($^\circ$)	ω ($^\circ$)	Ω ($^\circ$)	MA ($^\circ$)
PRO1	b	8.02	4.61694	0.059496	0.003547	4.97	48.39	17.47	129.43
PRO1	c	8.69	240.92	0.830939	0.254632	12.62	245.89	259.40	153.03
PRO1	d	10.05	1281.08	2.532293	0.274677	24.55	253.71	10.22	83.16
PRO2	b	1.78	4.61716	0.059408	0.011769	22.99	51.14	7.28	103.53
PRO2	c	10.78	241.02	0.831580	0.247042	10.09	248.74	256.34	154.47
PRO2	d	8.86	1282.57	2.533539	0.249090	28.30	253.27	9.97	82.57
PRO3	b	2.20	4.61726	0.059415	0.003972	18.41	44.98	17.09	148.28
PRO3	c	8.92	240.91	0.830954	0.247205	12.36	247.69	243.16	155.52
PRO3	d	9.92	1281.41	2.532645	0.302355	24.78	252.60	9.59	83.20
PRO4	b	2.81	4.61693	0.059421	0.021686	14.27	49.50	348.56	150.17
PRO4	c	9.01	240.93	0.831030	0.231669	12.31	244.39	243.47	154.06
PRO4	d	9.98	1280.56	2.531579	0.278130	24.74	252.37	9.90	83.77

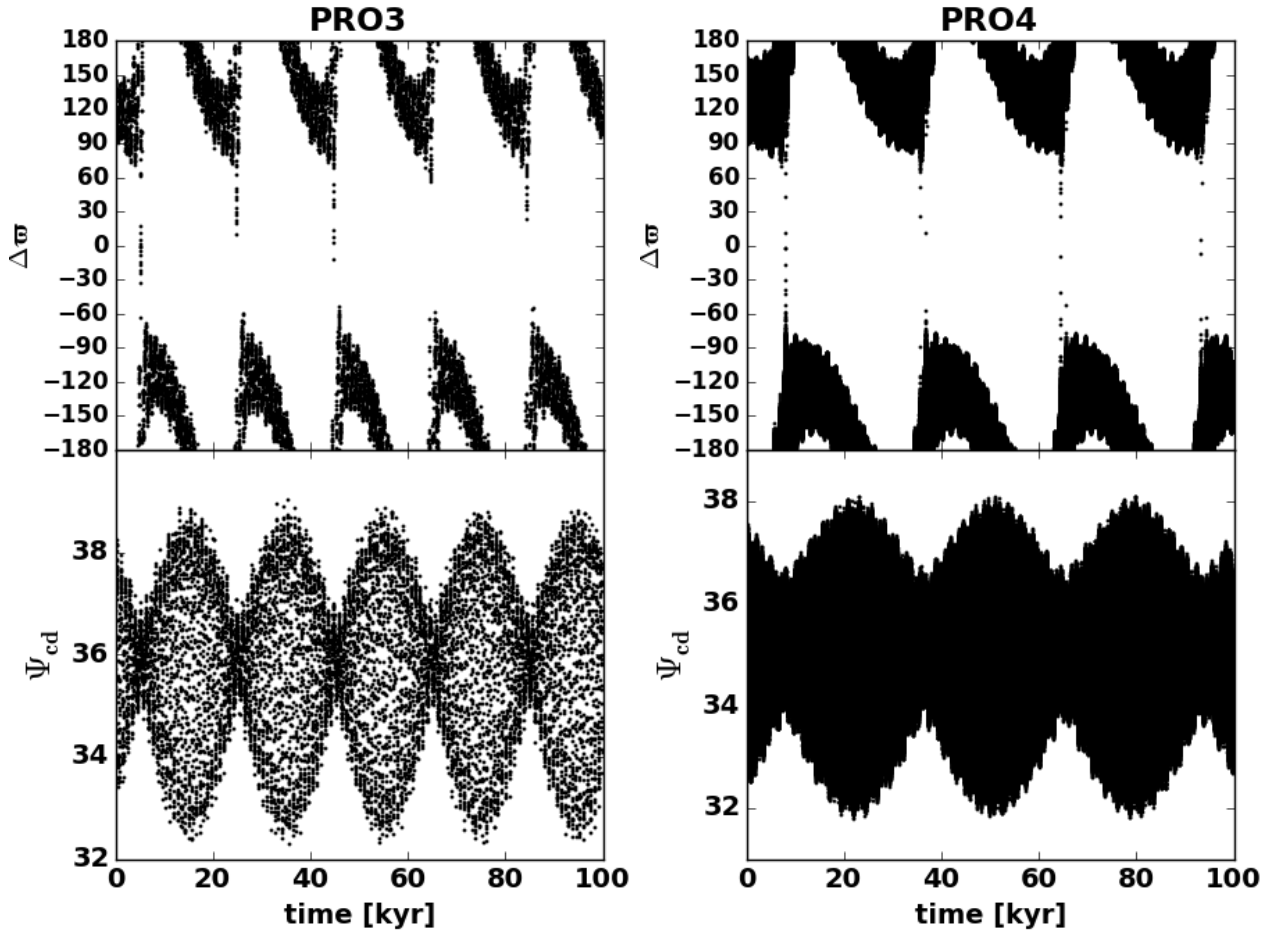


FIG. 8.— Secular behavior of planets c and d. $\Delta\varpi = \varpi_d - \varpi_c$ librates with intermittent circulation in both cases. **PRO4** is plotted with finer time resolution to show the circulation, which occurs very quickly. The mutual inclination, Ψ_{cd} , oscillates about $\sim 35^\circ$ in both cases with a $\sim 6^\circ$ amplitude.

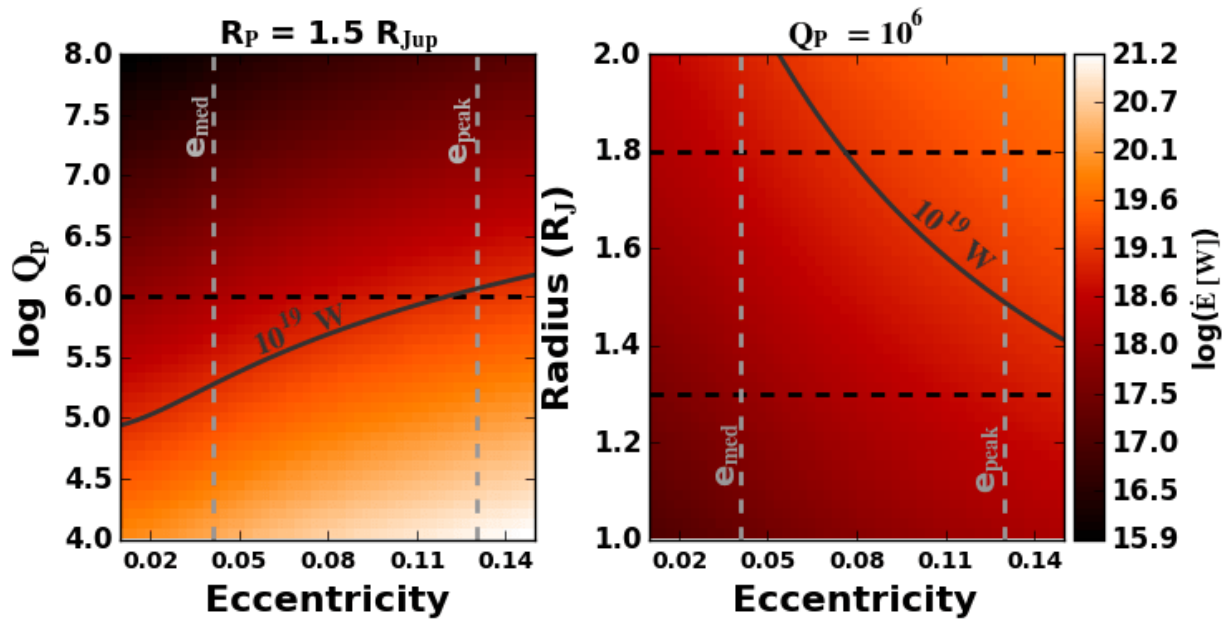


FIG. 9.— Tidal heating for v and b in case **PRO1**. Left: the equilibrium heating rate in Watts as a function of tidal quality factor, Q_p and eccentricity. The horizontal dashed line represents $Q_p = 10^6$, the value of Q_p in the right panel. Right: the equilibrium heating rate as a function of planet radius and eccentricity. Horizontal dashed lines represent the characteristic radii suggested by Crossfield et al. (2010) to explain the infrared phase curve. At $i_b = 14^\circ$, the planet must be $1.8 R_{Jup}$ to produce the observed variational amplitude, while at $i_b = 28^\circ$ it must be $1.3 R_{Jup}$. The vertical gray dashed lines represent the median and peak eccentricity of the planet, $e_{med} = 0.041$ and $e_{peak} = 0.13$. The gray curve indicates the heating rate predicted by Ibgui & Burrows (2009) for the planet HD 209458 b in the first two billion years of its tidal evolution. We find that v and b can have similar internal heating rates. Heating plots for **PRO2** and look very similar to those for **PRO1**.

REFERENCES

- Adams, F. C., & Laughlin, G. 2006, *ApJ*, 649, 992
 Aksnes, K., & Franklin, F. A. 2001, *AJ*, 122, 2734
 Baines, E. K., McAlister, H. A., ten Brummelaar, T. A., Turner, N. H., Sturmman, J., Sturmman, L., Goldfinger, P. J., & Ridgway, S. T. 2008, *ApJ*, 680, 728
 Barnes, R., & Greenberg, R. 2007a, *ApJ*, 659, L53
 —. 2007b, *ApJ*, 659, L53
 Barnes, R., Greenberg, R., Quinn, T. R., McArthur, B. E., & Benedict, G. F. 2011, *ApJ*, 726, 71
 Barnes, R., Mullins, K., Goldblatt, C., Meadows, V. S., Kasting, J. F., & Heller, R. 2013, *Astrobiology*, 13, 225
 Barnes, R., & Quinn, T. 2001, *ApJ*, 550, 884
 —. 2004, *ApJ*, 611, 494
 Barnes, R., & Raymond, S. N. 2004, *ApJ*, 617, 569
 Brogi, M., Snellen, I. A. G., de Kok, R. J., Albrecht, S., Birkby, J., & de Mooij, E. J. W. 2012, *Nature*, 486, 502
 Burrows, A., Budaj, J., & Hubeny, I. 2008, *ApJ*, 678, 1436
 Butler, R. P., Marcy, G. W., Fischer, D. A., Brown, T. M., Contos, A. R., Korzennik, S. G., Nisenson, P., & Noyes, R. W. 1999, *ApJ*, 526, 916
 Butler, R. P., Marcy, G. W., Williams, E., Hauser, H., & Shirts, P. 1997, *ApJ*, 474, L115
 Casertano, S. et al. 2008, *A&A*, 482, 699
 Chambers, J. E. 1999, *MNRAS*, 304, 793
 Chiang, E. I., Fischer, D., & Thommes, E. 2002, *ApJ*, 564, L105
 Chiang, E. I., & Murray, N. 2002, *ApJ*, 576, 473
 Chiang, E. I., Tabachnik, S., & Tremaine, S. 2001, *AJ*, 122, 1607
 Crossfield, I. J. M., Hansen, B. M. S., Harrington, J., Cho, J. Y.-K., Deming, D., Menou, K., & Seager, S. 2010, *ApJ*, 723, 1436
 Curiel, S., Cantó, J., Georgiev, L., Chávez, C. E., & Poveda, A. 2011, *A&A*, 525, A78
 Danby, J. M. A. 1988, *Fundamentals of celestial mechanics*
 Darwin, G. H. 1880, *Royal Society of London Philosophical Transactions Series I*, 171, 713
 Efroimsky, M., & Makarov, V. V. 2013, *ApJ*, 764, 26
 Ferraz-Mello, S., Rodríguez, A., & Hussmann, H. 2008, *Celestial Mechanics and Dynamical Astronomy*, 101, 171
 Fischer, D. A. et al. 2003, *ApJ*, 586, 1394
 Fischer, D. A., Marcy, G. W., & Spronck, J. F. P. 2014, *ApJS*, 210, 5
 Ford, E. B., Havlickova, M., & Rasio, F. A. 2001, *Icarus*, 150, 303
 Ford, E. B., Lystad, V., & Rasio, F. A. 2005, *Nature*, 434, 873
 Ford, E. B., & Rasio, F. A. 2008, *ApJ*, 686, 621
 François, P., Briot, D., Spite, F., & Schneider, J. 1999, *A&A*, 349, 220
 Goldreich, P., & Soter, S. 1966, *Icarus*, 5, 375
 Goździewski, K., Bois, E., Maciejewski, A. J., & Kiseleva-Eggleton, L. 2001, *A&A*, 378, 569
 Harrington, J., Hansen, B. M., Luszcz, S. H., Seager, S., Deming, D., Menou, K., Cho, J. Y.-K., & Richardson, L. J. 2006, *Science*, 314, 623
 Hartman, J. D. et al. 2011, *ApJ*, 742, 59
 Ibgui, L., & Burrows, A. 2009, *ApJ*, 700, 1921
 Ito, T., & Miyama, S. M. 2001, *ApJ*, 552, 372
 Jiang, I.-G., & Ip, W.-H. 2001, *A&A*, 367, 943
 Laughlin, G., & Adams, F. C. 1999, *ApJ*, 526, 881
 Libert, A.-S., & Henrard, J. 2007, *A&A*, 461, 759
 Libert, A.-S., & Tsiganis, K. 2011, *MNRAS*, 412, 2353
 Lissauer, J. J. 1999, *Nature*, 398, 659
 Lissauer, J. J., & Rivera, E. J. 2001, *ApJ*, 554, 1141
 Malbet, F. et al. 2012, *Experimental Astronomy*, 34, 385
 Malhotra, R. 2002, *ApJ*, 575, L33
 Mazeh, T., Zucker, S., dalla Torre, A., & van Leeuwen, F. 1999, *ApJ*, 522, L149
 McArthur, B. E., Benedict, G. F., Barnes, R., Martioli, E., Korzennik, S., Nelan, E., & Butler, R. P. 2010, *ApJ*, 715, 1203
 McArthur, B. E., Benedict, G. F., Henry, G. W., Hatzes, A., Cochran, W. D., Harrison, T. E., Johns-Krull, C., & Nelan, E. 2014, in press
 Michtchenko, T. A., Ferraz-Mello, S., & Beaugé, C. 2006, *Icarus*, 181, 555
 Michtchenko, T. A., & Malhotra, R. 2004, *Icarus*, 168, 237
 Migaszewski, C., & Goździewski, K. 2009, *MNRAS*, 392, 2
 Miller, N., Fortney, J. J., & Jackson, B. 2009, *ApJ*, 702, 1413
 Murray, C. D., & Dermott, S. F. 1999, *Solar system dynamics*
 Naef, D., Mayor, M., Beuzit, J. L., Perrier, C., Queloz, D., Sivan, J. P., & Udry, S. 2004, *A&A*, 414, 351
 Nagasawa, M., & Lin, D. N. C. 2005, *ApJ*, 632, 1140
 Nagasawa, M., Lin, D. N. C., & Ida, S. 2003, *ApJ*, 586, 1374
 Namouni, F. 2005, *AJ*, 130, 280
 Ogilvie, G. I., & Lin, D. N. C. 2004, *ApJ*, 610, 477
 Pourbaix, D. 2001, *A&A*, 369, L22
 Quirrenbach, A. 2010, in *Exoplanets*, ed. S. Seager (The University of Arizona Press)
 Rauch, K. P., & Hamilton, D. P. 2002, in *Bulletin of the American Astronomical Society*, Vol. 34, AAS/Division of Dynamical Astronomy Meeting #33, 938
 Reffert, S., & Quirrenbach, A. 2011, *A&A*, 527, A140
 Rivera, E., & Haghighipour, N. 2007, *MNRAS*, 374, 599
 Rivera, E. J., & Lissauer, J. J. 2000, *ApJ*, 530, 454
 Rodler, F., Lopez-Morales, M., & Ribas, I. 2012, *ApJ*, 753, L25
 Simpson, E. K., Baliunas, S. L., Henry, G. W., & Watson, C. A. 2010, *MNRAS*, 408, 1666
 Stepinski, T. F., Malhotra, R., & Black, D. C. 2000, *ApJ*, 545, 1044
 Takeda, G., Ford, E. B., Sills, A., Rasio, F. A., Fischer, D. A., & Valenti, J. A. 2007, *ApJS*, 168, 297
 Triard, A. H. M. J. et al. 2010, *A&A*, 524, A25
 Tuomi, M., Pinfield, D., & Jones, H. R. A. 2011, *A&A*, 532, A116
 Valenti, J. A., & Fischer, D. A. 2005, *ApJS*, 159, 141
 Van de Kamp, P. 1967, *Principles of Astrometry* (W. H. Freeman and Company)
 Veras, D., & Armitage, P. J. 2007, *ApJ*, 661, 1311
 Wisdom, J., & Holman, M. 1991, *AJ*, 102, 1528
 Wright, J. T., Upadhyay, S., Marcy, G. W., Fischer, D. A., Ford, E. B., & Johnson, J. A. 2009, *ApJ*, 693, 1084
 Yoder, C. F., & Peale, S. J. 1981, *Icarus*, 47, 1

APPENDIX

COMMENT ABOUT COORDINATES

There is a difference in the conventions used by dynamicists and observers to relate the longitude of ascending node, Ω , to the Cartesian coordinate system. Dynamicists and dynamical models typically use the convention that Ω is measured from the $+X$ -axis toward the $+Y$ -axis (see Murray & Dermott 1999), while observers typically measure Ω from the $+Y$ -axis (which typically corresponds to North, as in Van de Kamp 1967) toward the $+X$ -axis (typically East).

Because of this, if dynamicist's conventions are used to calculate the Cartesian coordinates of a planet's position based on the orbital elements (and these were intended for use by an observer), these coordinates would not correspond to the actual position of the planet on the sky, relative to its host star. Rather, the X and Y positions would be swapped. The reason for this can be easily understood by comparing the equations for X and Y from Van de Kamp (1967) and those from Murray & Dermott (1999).

Van de Kamp (1967) has:

$$X_{obs} = B \frac{x}{a} + G \frac{y}{a} \quad (A1)$$

$$Y_{obs} = A \frac{x}{a} + F \frac{y}{a}, \quad (A2)$$

where x and y are the positions of the planet in its own orbital plane, X_{obs} and Y_{obs} are the positions of the planet on

the sky, using observer's conventions, and A , B , F , and G (the Thiele-Innes constants) are:

$$A = a(\cos \omega \cos \Omega - \sin \omega \sin \Omega \cos i) \quad (\text{A3})$$

$$B = a(\cos \omega \sin \Omega + \sin \omega \cos \Omega \cos i) \quad (\text{A4})$$

$$F = a(-\sin \omega \cos \Omega - \cos \omega \sin \Omega \cos i) \quad (\text{A5})$$

$$G = a(-\sin \omega \sin \Omega + \cos \omega \cos \Omega \cos i).. \quad (\text{A6})$$

On the other hand, Murray & Dermott (1999) have:

$$\begin{aligned} X_{dyn} = & x(\cos \Omega \cos \omega - \sin \Omega \sin \omega \cos i) \\ & - y(\cos \Omega \sin \omega + \sin \Omega \cos \omega \cos i) \end{aligned} \quad (\text{A7})$$

$$\begin{aligned} Y_{dyn} = & x(\sin \Omega \cos \omega + \cos \Omega \sin \omega \cos i) \\ & - y(\sin \Omega \sin \omega + \cos \Omega \cos \omega \cos i), \end{aligned} \quad (\text{A8})$$

$$(\text{A9})$$

where X_{dyn} and Y_{dyn} are the positions of the planet on the sky, using dynamicist's conventions. Equations A7 and A8 can be rewritten,

$$X_{dyn} = A \frac{x}{a} + F \frac{y}{a} \quad (\text{A10})$$

$$Y_{dyn} = B \frac{x}{a} + G \frac{y}{a}. \quad (\text{A11})$$

Comparing Equations A10 and A11 with A1 and A2, we can see that $X_{dyn} = Y_{obs}$ and $Y_{dyn} = X_{obs}$. This means that in a dynamical model, the orbit will be a mirror image of the true observed orbit, if the observed orbital elements are taken at face value (see Figure 10). This point is subtle, but can lead to spurious results if an observer uses the Cartesian coordinates from an orbital simulation to plan future observations. If all observations and simulations are performed using orbital elements with their respective conventions, then all results should be consistent.

This consistency is possible because the reflection has no impact on the dynamics of the system, because all planets' orbits will be reflected about the same plane, so all relative positions and velocities are preserved, and the energy (which is a function of the semi-major axes) and angular momentum (a function of semi-major axis and eccentricity) are the same in the mirror image system as in the true system. Thus, as long as communication of planetary properties between observers and dynamicists is restricted to Keplerian orbital elements, there should be no difficulty in correctly modeling an observed system or in making predictions of planetary positions for future observations.

One should bear in mind the difference in Cartesian coordinates, however, when combining observational and dynamical techniques, and pass only orbital elements between models or take into account the X/Y swap if necessary.

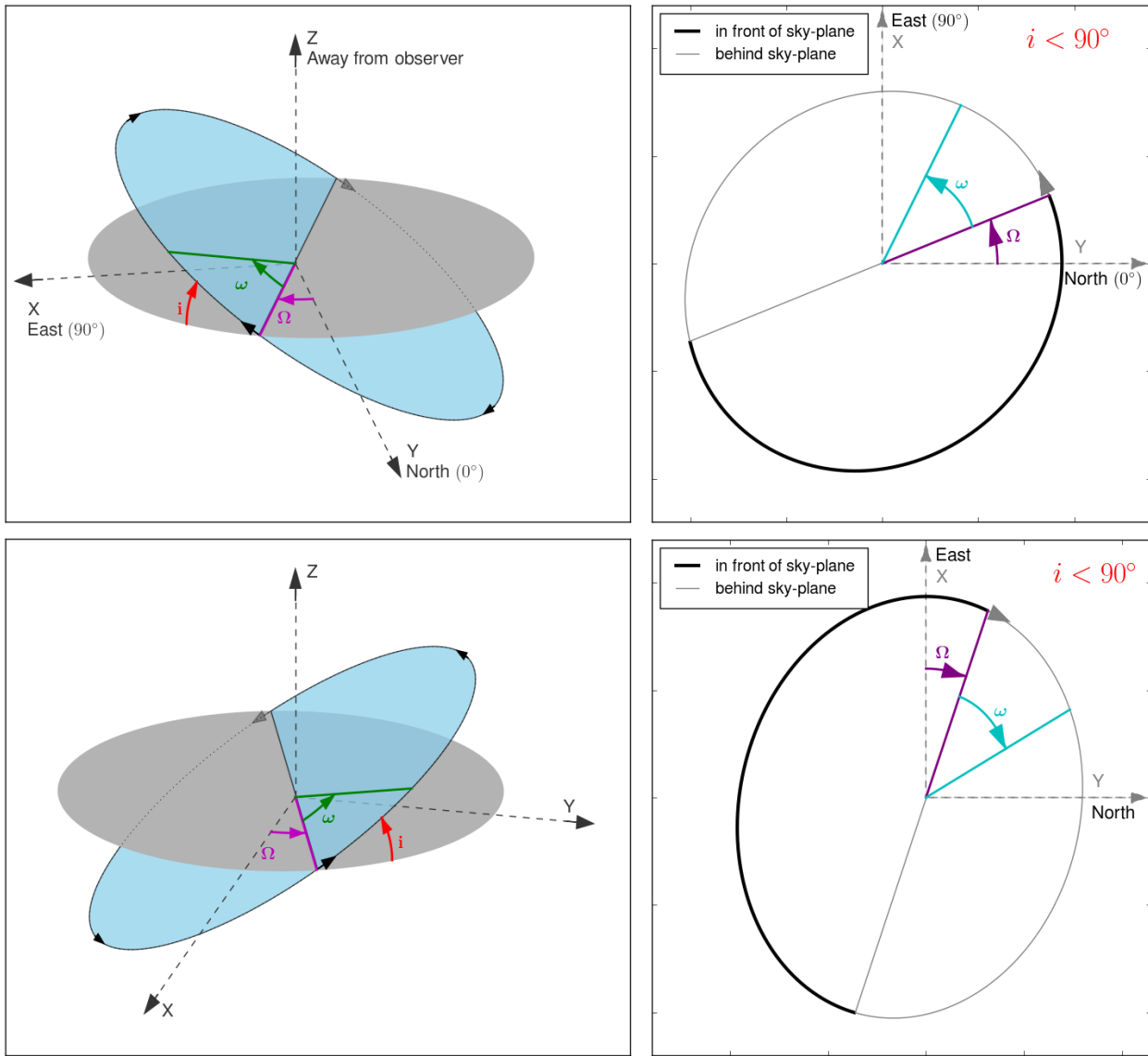


FIG. 10.— A comparison of the orbits produced in calculating Cartesian coordinates using “observer” conventions and “dynamicist” conventions. Upper left: 3D projection of the observer’s orbit, from Van de Kamp (1967). Ω is measured from the Y-axis (North) toward the X-axis (East). Upper right: The observer’s orbit, projected on the sky. Ω is measured counterclockwise from the Y-axis (North). Lower left: 3D projection of the dynamicist’s orbit. Ω is measured from the X-axis toward the Y-axis, which causes the X and Y coordinates of the planet to be swapped compared to the (true) observer’s orbit. Lower right: The dynamicist’s orbit, projected on the sky. Again, the X and Y coordinates of the planet in its orbit will be swapped compared to the observer’s orbit.